

MeV-GeV emission from neutron-loaded short gamma-ray burst jets

Soebur Razzaque and Peter Mészáros

Department of Astronomy & Astrophysics, Department of Physics, Pennsylvania State University, University Park, PA 16802
soeb@astro.psu.edu, nnp@astro.psu.edu

ABSTRACT

Recent discovery of the afterglow emission from short gamma-ray bursts suggests that binary neutron star or black hole-neutron star binary mergers are the likely progenitors of these short bursts. The accretion of neutron star material and its subsequent ejection by the central engine implies a neutron-rich outflow. We consider here a neutron-rich relativistic jet model of short bursts, and investigate the high energy neutrino and photon emission as neutrons and protons decouple from each other. We find that upcoming neutrino telescopes are unlikely to detect the 50 GeV neutrinos expected in this model. For bursts at $z \sim 0.1$, we find that *GLAST* and ground-based Cherenkov telescopes should be able to detect prompt 100 MeV and 100 GeV photon signatures, respectively, which may help test the neutron star merger progenitor identification.

Subject headings: gamma rays: bursts—gamma rays: theory—ISM: jets and outflows—radiation mechanisms: non thermal—stars: neutron

1. Introduction

The nature and origin of short gamma-ray bursts (SGRBs), with $t_\gamma \lesssim 2$ s duration, were largely conjectural until recently. This changed dramatically with the detection of the afterglow and the identification of the host galaxy of GRB 050509b at a redshift $z = 0.226$ (Gehrels, et al. 2005), as well as subsequent observations of other short burst afterglows, e.g., GRB 050709 (Fox, et al. 2005; Villasenor, et al. 2005), GRB 050724 (Barthelmy et al. 2005), etc. These observations revealed that the short bursts are located mainly in elliptical hosts, while some are in spirals or irregulars, as expected from an old population such as NS-NS or NS-BH mergers. They also provided, for the first time, details about the X-ray, and in some cases optical and radio afterglow lightcurves, including in two cases evidence

for a jet break, qualitatively similar to the relativistic jet afterglows of long GRBs [see, e.g., Zhang & Mészáros (2004) for reviews of long GRBs]. The average redshifts are lower than for long bursts, indicating an isotropic-equivalent energy of SGRBs approximately two orders of magnitude lower than for long ones.

We investigate here a model of SGRB jet which is initially loaded with neutrons and fewer protons, as expected from a neutron star composition. High energy emission in this model is then expected from the photosphere of the relativistic jet outflow, including both thermal and non-thermal components, in addition to the radiation expected outside of it. We describe our jet model in Section 2, high energy emission processes in Section 3, and expected neutrino and photon fluxes in Section 4 and 5 respectively. We summarize and discuss our results in Section 6.

2. Neutron loaded jet dynamics

We assume the total isotropic-equivalent energy outflow in the SGRB jet of $L = 10^{50} L_{50}$ erg/s. The jet is loaded with protons and neutrons with an initial neutron to proton number density ratio $\xi_o = n'_n/n'_p = 10\xi_{o,1}$ in the comoving frame.¹ The total mass outflow rate in such a neutron-rich jet is $\dot{M} = 4\pi r^2 c(1 + \xi_o)n'_p m_p$ initially, since $m_p \simeq m_n \gg m_e$ and the thermal energy is negligible. A useful quantity is the usual total energy to mass flow ratio $\eta = L/\dot{M}c^2$, characterizing the dimensionless entropy or the baryon loading of the jet. In a typical long GRB ($t_\gamma \gtrsim 2$ s) the final bulk Lorentz factor of the γ -ray emitting fireball is equivalent to η . In the case of SGRBs, we assume $\eta = 316\eta_{2.5}$, similar to that of the long GRBs, motivated by observation.

The outflow starts at a radius $R_o = 10^6 R_{o,6}$ cm which is a few times the Schwarzschild radius $r_g = 2GM_{\text{bh}}/c^2$ of a solar mass black hole created by binary mergers. The initial temperature of the plasma outflow is

$$T'_o = \left(\frac{L}{4\pi R_o^2 c a} \right)^{1/4} \approx 1.2 \left(\frac{L_{50}}{R_{o,6}^2} \right)^{1/4} \text{ MeV}, \quad (1)$$

where $a = \pi^2 k^4 / 15(\hbar c)^3 = 7.6 \times 10^{-15}$ erg cm⁻³ K⁻⁴ is the radiation density constant. The optically thick hot plasma expands adiabatically due to the radiation pressure. The comoving temperature drops as $T'(r) \propto R_o/r$ and the plasma expands with an increasing bulk Lorentz factor $\Gamma(r) \propto r/R_o$ with the radius r following the adiabatic law. Electrons (both e^\pm and

¹We use primed variables in the relativistic plasma frame and un-primed variables in the observer frame or laboratory frame

$n_e \simeq n_p$) are coupled to the photons via Compton scattering, and protons, which are coupled to the electrons via Coulomb interaction, are held together in the expanding optically thick plasma. Neutrons, however, are somewhat loosely coupled to the protons by elastic nuclear scattering with a cross-section $\sigma_{np} \approx 3 \times 10^{-26} \text{ cm}^2$, which is roughly a fraction 1/20 of the Thomson cross-section ($\sigma_{\text{Th}} \approx 6.65 \times 10^{-25} \text{ cm}^2$). This changes considerably the dynamics of a neutron-rich jet [e.g. Derishev, Kocharovskiy & Kocharovskiy (1999); Bahcall & Mészáros (2000); Beloborodov (2003)] as we discuss next.

The protons and neutrons are coupled together with a common bulk Lorentz factor $\Gamma_n(r) \simeq \Gamma_p(r) \simeq \Gamma(r)$ as long as the n - p collision time $t'_{np} \simeq (n'_p \sigma_{np} c)^{-1}$ is shorter than the plasma expansion time $t'_{\text{exp}} \simeq r/c\Gamma(r)$. The critical dimensionless entropy for which n - p decoupling happens, from the condition $t'_{np} = t'_{\text{exp}}$, is

$$\eta_{np} \simeq \left[\frac{L\sigma_{np}}{4\pi R_o m_p c^3 (1 + \xi_o)} \right]^{1/4} \approx 150 \left[\frac{L_{50}}{R_{o,6} (1 + \xi_{o,1})} \right]^{1/4}. \quad (2)$$

As a result, the neutrons and protons in our SGRB jet model ($\eta \gtrsim \eta_{np}$) decouple at a radius where the nuclear scattering optical depth $\tau'_{np} \simeq n'_p \sigma_{np} R_{np} / \Gamma(R_{np}) = 1$ as

$$R_{np} \simeq \left[\frac{L\sigma_{np}}{4\pi R_o \eta m_p c^3 (1 + \xi_o)} \right]^{1/3} R_o = \eta_{np} \left(\frac{\eta_{np}}{\eta} \right)^{1/3} \approx 1.2 \times 10^8 \left[\frac{L_{50} R_{o,6}^2}{\eta_{2.5} (1 + \xi_{o,1})} \right]^{1/3} \text{ cm}. \quad (3)$$

The bulk Lorentz factor of the neutrons does not increase further and saturates to a final value of

$$\Gamma_{n,f} = \frac{R_{np}}{R_o} \approx 115 \left[\frac{L_{50}}{\eta_{2.5} R_{o,6} (1 + \xi_{o,1})} \right]^{1/3}, \quad (4)$$

at $r = R_{np}$. The neutrons start to lag behind the protons at $r \gtrsim R_{np}$, and the total energy outflow due to protons is

$$\hat{L} = L - \Gamma_{n,f} \hat{M} c^2 \xi_o = L \left(1 - \frac{\Gamma_{n,f}}{\eta} \frac{\xi_o}{1 + \xi_o} \right) \approx 7 \times 10^{49} \text{ ergs/s}, \quad (5)$$

which is close to the initial value of L since $\Gamma_{n,f} < \eta$. Here $\hat{M} \simeq \dot{M}/(1 + \xi_o)$ is the proton mass outflow rate after decoupling. The outflow is still optically thick at $r = R_{np}$ since $\sigma_{\text{Th}} \simeq 20\sigma_{np}$. The decoupling of radiation from plasma electrons takes place for a critical value for the dimensionless entropy, for which the Thomson scattering time scale $t'_{\text{Th}} \simeq (n'_e \sigma_{\text{Th}} c)^{-1}$ is equal to the plasma expansion time, is given by

$$\hat{\eta}_{\text{rad}} = \left(\frac{\hat{L}\sigma_{\text{Th}}}{4\pi R_o m_p c^3} \right)^{1/4} \approx 530 \left(\frac{\hat{L}_{49.8}}{R_{o,6}} \right)^{1/4}, \quad (6)$$

for our SGRB parameter $\hat{L}_{49.8} = \hat{L}/(7 \times 10^{49} \text{ ergs/s})$. Note that the dimensionless entropy of the proton outflow $\hat{\eta} \equiv \hat{L}/\hat{M}c^2$ is related to $\hat{\eta}_{\text{rad}}$ by

$$\frac{\hat{\eta}}{\hat{\eta}_{\text{rad}}} \simeq \left[1 + \xi_o \left(1 - \frac{\Gamma_{n,f}}{\eta} \right) \right]^{3/4} \left(\frac{\sigma_{np}}{\sigma_{\text{Th}}} \right)^{1/4} \frac{\eta}{\eta_{np}} \approx 4.4. \quad (7)$$

In this case ($\hat{\eta} > \hat{\eta}_{\text{rad}}$) the outflow becomes transparent during the acceleration phase $\Gamma \propto r$, at a radius $r = R_\tau$ where the Thomson optical depth $\tau'_{\text{Th}} \simeq n'_e R_\tau / \Gamma(R_\tau) = 1$,

$$R_\tau \simeq R_o \hat{\eta}_{\text{rad}} \left(\frac{\hat{\eta}_{\text{rad}}}{\hat{\eta}} \right)^{1/3} \approx 3.2 \times 10^8 \text{ cm}, \quad (8)$$

which is close to R_{np} . The final Lorentz factor of the (proton) outflow is given by (Rossi, Beloborodov & Rees 2005)

$$\Gamma_{p,f} \simeq \hat{\eta}_{\text{rad}} \left(\frac{\hat{\eta}}{\hat{\eta}_{\text{rad}}} \right)^{1/9} \approx 624 \quad (9)$$

which is achieved at a radius $r \sim R_\tau$ for this η . This suggests a possible way to generate the high bulk Lorentz factor estimated in short GRBs without any spectral lags in the data (Norris & Bonnell 2006).

Note that for $\eta < \eta_{np}$, one has $\Gamma_{n,f} = \Gamma_{p,f} = \eta$ for a baryon loaded jet outflow satisfying the condition $\eta < \eta_{\text{rad}}$. Here η_{rad} is the initial critical radiation entropy for combined proton and neutron outflow, defined with an equation similar to equation (6) as

$$\eta_{\text{rad}} = \left[\frac{L\sigma_{\text{Th}}}{4\pi R_o m_p c^3 (1 + \xi_o)} \right]^{1/4} \approx 322 \left[\frac{L_{50}}{R_{o,6} (1 + \xi_{o,1})} \right]^{1/4} \quad (10)$$

We have plotted the final proton and neutron bulk Lorentz factors as functions of the baryon-loading parameter in Figure 1. For a given total energy outflow rate L , the maximum allowed value of η , from equation (10), are shown as three vertical solid lines for three values of initial neutron to proton ratio $\xi_o = 1, 5$ and 10. Note that for $\eta \sim 316\eta_{2.5}$, a typical value used for long GRB modelling, the neutron and proton components always decouple [see equation (2)] in case of SGRBs because of a lower L . On the contrary, n - p decouple only for $\xi_o \gtrsim 4$ in case of a long GRB with $\eta \sim 316\eta_{2.5}$, $L = 10^{52} L_{52} \text{ erg/s}$ and $R_o = 10^7 R_{o,7} \text{ cm}$. Also note the high $\Gamma_{p,f}$ values of 519, 572 and 624 for $\xi_o = 1, 5$ and 10 respectively in Figure 1 from equation (9).

3. Inelastic neutron-proton scattering

The elastic component of the total np cross-section, which dominates at lower energy, drops rapidly above the pion production threshold of $\approx 140 \text{ MeV}$, where the inelastic np

scattering cross-section is $\sigma_\pi \approx \sigma_{np}$. Hence, the condition $\eta \gtrsim \eta_{np}$ (and subsequently $\hat{\eta} \gtrsim \hat{\eta}_{\text{rad}}$) for n - p decoupling implies that there will be pion production by the threshold processes, with roughly equal (total unit) probability to produce a π^\pm pair or (and) $2\pi^0$,

$$pn \rightarrow \begin{cases} nn\pi^+ ; \pi^+ \rightarrow \mu^+\nu_\mu \rightarrow e^+\nu_e\bar{\nu}_\mu\nu_\mu \\ pp\pi^- ; \pi^- \rightarrow \mu^-\bar{\nu}_\mu \rightarrow e^-\bar{\nu}_e\nu_\mu\bar{\nu}_\mu \\ pn\pi^0 ; \pi^0 \rightarrow \gamma\gamma \end{cases} \quad (11)$$

The secondary pions produced by the inelastic np scattering are at rest in the center-of-mass (c.m.) frame of interaction. However, the neutrons are not cold in the comoving outflow frame as we discuss next, and the c.m. frame acquires a velocity relative to this frame.

The Lorentz factor of the neutrons relative to the outflowing protons, at the radius $r \sim R_\tau \sim R_{np}$, is given by

$$\Gamma_{\text{rel}} = \Gamma_p\Gamma_n(1 - \beta_p\beta_n) \simeq \frac{1}{2} \left(\frac{\Gamma_{p,f}}{\Gamma_{n,f}} + \frac{\Gamma_{n,f}}{\Gamma_{p,f}} \right) \approx 2.8 \quad (12)$$

Thus, in (proton) outflow rest frame the neutron energy is $\epsilon'_n = \Gamma_{\text{rel}}m_n c^2$ and the Lorentz factor of the c.m. is given by $\gamma'_{\text{c.m.}} = (\epsilon'_n + m_p c^2)/(m_p^2 c^4 + m_n^2 c^4 + 2\epsilon'_n m_p c^2)^{1/2} \approx 1.4$. The energies of the decay neutrinos are $\epsilon'_{\nu_\mu} \simeq \epsilon'_{\bar{\nu}_\mu} \approx 30\gamma'_{\text{c.m.}}$ MeV from π^\pm , $\epsilon'_{\nu_e} \simeq \epsilon'_{\bar{\nu}_e} \approx 30\gamma'_{\text{c.m.}}$ MeV and $\epsilon'_{\nu_\mu} \simeq \epsilon'_{\bar{\nu}_\mu} \approx 50\gamma'_{\text{c.m.}}$ MeV from μ^\pm . The π^0 decay photon energy is $\epsilon'_\gamma \approx 70\gamma'_{\text{c.m.}}$ MeV. The observed energies of the decay products would be

$$\epsilon = \epsilon'\Gamma_{p,f} = \begin{cases} 26 \text{ GeV} ; (\nu_\mu \text{ and } \nu_e \text{ from } \pi^\pm \text{ and } \mu^\pm) \\ 43 \text{ GeV} ; (\nu_\mu \text{ from } \mu^\pm) \\ 60 \text{ GeV} ; (\gamma) \end{cases} \times \Gamma_{p,2.8}. \quad (13)$$

Here $\Gamma_{p,2.8} = \Gamma_{p,f}/624$.

Note that additional pions may be produced via $pp \rightarrow pn\pi^+$ and $nn \rightarrow np\pi^-$ inelastic interactions with similar cross-sections as the inelastic np interaction. The nn process in particular may be important for neutron destruction in the outflow (Rossi, Beloborodov & Rees 2005). Neutrinos and photons produced from nn and pp processes, however, are of much lower energy as the relative velocities between the n - n or p - p components (e.g., arising from a variable outflow) may not exceed that between n - p in equation (12).

4. Neutrino emission

The inelastic n - p scattering opacity is $\tau'_\pi \simeq \tau'_{np} \simeq 1$ at $r \sim R_{np} \sim R_\tau$ and each proton produces, on average, a π^\pm pair half of the time. The decay neutrinos escape the plasma

outflow as soon as they are created. The neutrino and anti-neutrino flux rate from an SGRB at $z \simeq 0.1$ (corresponding to a luminosity distance $D_L \simeq 10^{27} D_{27}$ cm for a standard cosmology with Hubble constant $H_o \simeq 70 \text{ km s}^{-1} \text{ Mpc}^{-1}$) is

$$\dot{N}_{\nu_\mu} \simeq \dot{N}_{\bar{\nu}_\mu} \simeq 2\dot{N}_{\nu_e} \simeq 2\dot{N}_{\bar{\nu}_e} \simeq \frac{\hat{L}}{4\pi D_L^2 \Gamma_{p,f} m_p c^2} \approx 5.7 \times 10^{-6} \frac{\hat{L}_{49.8}}{D_{27}^2 \Gamma_{p,2.8}} \text{ cm}^{-2} \text{ s}^{-1}. \quad (14)$$

The neutrino-nucleon (νN) total cross-section for detection is $\sigma_{\nu N} \approx 6 \times 10^{-37} \text{ cm}^2$ at $\epsilon_\nu \approx 60 \text{ GeV}$ [see, e.g., Table 1. in Gandhi, et al. (1998)]. Upcoming kilometer scale water Cherenkov detectors such as *ANTARES* and *KM3NeT* are designed to have sensitivity for detecting neutrinos of energy $\gtrsim 50 \text{ GeV}$. The total number of nucleons in a gigaton detector is $N_N \approx 1.2 \times 10^{39}$, which folded with the cross-section and muon neutrino flux from a typical SGRB at $z \sim 0.1$ yields an event rate of

$$\dot{N}(\nu_\mu + \bar{\nu}_\mu \text{ event}) \simeq 2\dot{N}_{\nu_\mu} \sigma_{\nu N} N_N \approx 0.01 \hat{L}_{49.8} D_{27}^{-2} \Gamma_{p,2.8}^{-1} \text{ s}^{-1} \text{ Gton}^{-1} \quad (15)$$

per burst. Hence it is unlikely that upcoming neutrino telescopes would be able to detect these neutrinos, based on our model as discussed here, from individual SGRBs. The number of events from diffuse flux can be calculated assuming a burst rate of $\sim 300/4\pi \text{ yr}^{-1} \text{ sr}^{-1}$ (approximately 30% of the long GRB rate) distributed over the whole sky and an optimistic $2\pi \text{ sr}$ angular sensitivity of the detector as $(300/4\pi) \times 2\pi \times \dot{N}(\nu_\mu + \bar{\nu}_\mu \text{ event}) t \approx 1 \text{ yr}^{-1}$. Here, we have assumed $t \sim 1 \text{ s}$ as the typical duration of the SGRBs.

5. Photon emission

The γ -ray emission from an SGRB, however, is more promising. Although the plasma outflow becomes transparent to Compton scattering at a radius $r \sim R_\tau \sim R_{np} \sim 10^8 \text{ cm}$, not all the high energy photons due to π^0 decay can escape. Only those created below a skin depth of R_τ escape with a probability (Bahcall & Mészáros 2000)

$$P_{\pi^0} \simeq \tau'_{np}(R_\tau) \simeq R_{np}/R_\tau \approx 0.4. \quad (16)$$

The corresponding number flux of 60 GeV π^0 -decay photons at Earth is

$$\dot{N}_{\gamma,\pi^0} \simeq \frac{P_{\pi^0} \hat{L}}{4\pi D_L^2 \Gamma_{p,f} m_p c^2} \approx 2.0 \times 10^{-6} \frac{\hat{L}_{49.8}}{D_{27}^2 \Gamma_{p,2.8}} \text{ cm}^{-2} \text{ s}^{-1}, \quad (17)$$

which is below the detection threshold of *GLAST* “Large Area Telescope” (LAT), whose effective area is $\sim 10^4 \text{ cm}^2$ in this energy range (Gehrels & Michelson 1999). However,

ground-based Cherenkov telescopes with $\lesssim 100$ GeV threshold may detect these photons. In particular, *Milagro* has an effective area of $\sim 5 \times 10^5$ cm² for a zenith angle $\lesssim 15^\circ$ in this energy range (Dingus 2004). For a yearly SGRB rate of $\sim 300/\text{yr}$, this implies a possible detection rate of $\lesssim 5 \text{ yr}^{-1}$, assuming a 90% duty cycle.

The high energy photons from π^0 -decay created below R_τ interact with thermal photons of energy $\epsilon'_{\gamma,t} \simeq T'_o(R_o/R_\tau) \approx 3.6$ keV, which are carried along with the plasma. The number density of these photons is high, and all π^0 -decay photons of energy $\epsilon'_{\gamma,i} \approx 100$ MeV originating below the $\tau'_{\text{Th}} \sim 1$ skin depth produce e^\pm pairs satisfying the condition $\epsilon'_{\gamma,t}\epsilon'_{\gamma,i} \gtrsim m_e^2 c^4$. Assuming equal energy distribution among final particles, charged pion decay e^\pm and $\gamma\gamma \rightarrow e^\pm$ have a characteristic energy $\sim 35\gamma'_{\text{c.m.}}$ MeV, and initiate electromagnetic cascades by inverse-Compton (IC) scattering of thermal photons, creating new generations of pairs which interact again with the thermal photons. Contrary to the optically thick case of $\tau'_{\text{Th}} \gg 1$, where all upscattered photons are absorbed by thermal photons producing e^\pm pairs, these cascades are not saturated (Derishev, Kocharovsky & Kocharovsky 1999). The upscattered photons eventually escape from the photosphere with characteristic energy $\epsilon'_{\gamma,c} \approx m_e c^2$ below the e^\pm pair production threshold energy.

The fraction of the π^\pm and π^0 energy carried by the escaping γ -rays depends on the details. An order of magnitude estimate for this fraction is $\xi_\gamma = 0.1\xi_{\gamma,-1}$ (Rossi, Beloborodov & Rees 2005). Thus, the number flux of the escaping γ -rays of energy

$$\epsilon_{\gamma,c} \simeq \Gamma_{p,f} m_e c^2 \approx 320 \Gamma_{p,2.8} \text{ MeV} \quad (18)$$

at Earth is

$$\dot{N}_{\gamma,c} \simeq \frac{4\hat{L}}{4\pi D_L^2 \Gamma_{p,f} m_p c^2} \left(\xi_\gamma \frac{\gamma'_{\text{c.m.}} m_\pi c^2}{m_e c^2} \right) \approx 8.6 \times 10^{-4} \frac{\hat{L}_{49.8} \xi_{\gamma,-1}}{D_{27}^2 \Gamma_{p,2.8}} \text{ cm}^{-2} \text{ s}^{-1}. \quad (19)$$

The escaping Comptonized photon spectrum of the cascade is $dN_\gamma/d\epsilon_\gamma \propto \epsilon_\gamma^{-q}$, where $q \approx 5/3$ for $\epsilon_\gamma < \epsilon_{\gamma,c}$ and $q \approx 2.2$ for $\epsilon_{\gamma,c} < \epsilon_\gamma < \epsilon_{\gamma,\text{max}}$ (Belyanin and Derishev 2001). The maximum photon energy is $\epsilon_{\gamma,\text{max}} \simeq \gamma_e'^2 \epsilon'_{\gamma,t} \Gamma_{p,f} \approx 20$ GeV. The fluence threshold for *GLAST* is $\sim 4 \times 10^{-8}$ ergs cm⁻² for a short integration time (Gehrels & Michelson 1999). Thus the Comptonized photon fluence $\epsilon_{\gamma,c} F_{\epsilon_{\gamma,c}} \simeq \epsilon_{\gamma,c} \dot{N}_{\gamma,c} t \approx 4.4 \times 10^{-7}$ ergs cm⁻² for a typical SGRB of $t \sim 1$ s duration at $z \sim 0.1$ should be detectable by *GLAST* (see Figure 2).

Apart from the π^0 -decay photons of energy 60 GeV and e^\pm pair cascade photons of energy 320 MeV, the spectrum of radiation from the photosphere of an SGRB would also contain thermal photons of peak energy $\epsilon_{\gamma,b} \approx 2.82\epsilon'_{\gamma,t} \Gamma_{p,f} \approx 6.4\Gamma_{p,2.8}$ MeV (see Figure 2). The corresponding number flux on Earth of these photospheric photons of peak energy is

$$\dot{N}_{\gamma,b} \simeq \frac{\hat{L}}{4\pi D_L^2 \epsilon_{\gamma,b}} \approx 0.5 \frac{\hat{L}_{49.8}}{D_{27}^2 \Gamma_{p,2.8}} \text{ cm}^{-2} \text{ s}^{-1}. \quad (20)$$

The photon fluxes at various energies discussed above are associated with the jet photosphere, and last as long as the usual burst prompt γ -ray emission. Hence, these emissions would be contemporaneous with the emission at \sim MeV associated with internal shocks or other dissipation processes above the photosphere, aside from a small time lag between the onset of the two events of the order of a millisecond. We discuss emission from internal shocks next.

5.1. Comparison with internal shock emission

The internal shock model of plasma shells colliding at some radius above the photosphere is the most commonly discussed mechanism to produce the observed γ -rays in the fireball shock model. The average bulk Lorentz factor of the colliding shells is $\Gamma_i \simeq \Gamma_{p,f} \approx 624\Gamma_{i,2.8}$. With a millisecond variability time $t_v = 10^{-3}t_{v,-3}$ s, the internal shocks take place at a radius $r_i \simeq 2\Gamma_i^2 ct_v \approx 2.3 \times 10^{13}$ cm. Note that this is much smaller than the β -decay radius $\sim 3.4 \times 10^{15}$ cm. Hence, most neutrons have not had time to decay until well beyond the internal shock radius.

The equipartition magnetic field in the shock region is $B = (2\varepsilon_B \hat{L}/r_i^2 c)^{1/2} \approx 9.1 \times 10^5$ G with an equipartition fraction $\varepsilon_B = 0.1\varepsilon_{B,-1}$. The shock-accelerated electrons are assumed to follow a power-law energy distribution $dN'_e/d\gamma'_e \propto \gamma'^{-\alpha}$ for $\gamma'_e \geq \gamma'_{e,\min} \simeq \varepsilon_e m_p/m_e$ with $\alpha \approx 2.4$, which results in synchrotron radiation with a peak energy

$$\epsilon_{\gamma,m} = \hbar c \Gamma_i \frac{3\gamma'_{e,\min} e B}{2m_e c^2} \approx 330 \left(\frac{\varepsilon_{e,-1}^2 \varepsilon_{B,-1} \hat{L}_{49.8}}{\Gamma_{i,2.8}^2 t_{v,-3}^2} \right)^{1/2} \text{ keV}. \quad (21)$$

Here $\varepsilon_e = 0.1\varepsilon_{e,-1}$ is the fraction of fireball's kinetic energy transferred to the electrons by shocks. The corresponding number flux at Earth of these peak synchrotron photons is

$$\dot{N}_{\gamma,m} \simeq \frac{\hat{L}\varepsilon_e}{4\pi D_L^2 \epsilon_{\gamma,m}} \approx 1.0 \left(\frac{\hat{L}_{49.8} \Gamma_{i,2.8}^2 t_{v,-3}^2}{D_{27}^4 \varepsilon_{B,-1}} \right)^{1/2} \text{ cm}^{-2} \text{ s}^{-1}. \quad (22)$$

The typical synchrotron radiation spectrum from power-law distributed electron energy is $dN_\gamma/d\epsilon_\gamma \propto \epsilon_\gamma^{-(\alpha+2)/2} \sim \epsilon_\gamma^{-2.2}$ for $\epsilon_\gamma > \epsilon_{\gamma,m}$ (see Figure 2). The observed typical GRB spectra $dN_\gamma/d\epsilon_\gamma \propto \epsilon_\gamma^{-1}$, is slightly different from the theoretical synchrotron spectrum with an index $-3/2$.

We have plotted the energy spectra of synchrotron radiation from the internal shocks, and thermal and IC cascades from the jet photosphere in Figure 2. We used $L = 10^{50} L_{50}$ erg/s, $R_o = 10^6$ cm and $\eta = 316$ for all curves and $\xi_o = 1, 5$ and 10 for the dashed, dotted

and dotted-dash curves respectively. The peak energy of thermal photons ($\epsilon_{\gamma,b}$) decreases from 6.4 keV for $\xi_o = 10$ to 3 keV for $\xi_o = 1$ as the photosphere radius (R_τ) in equation (8) increases with decreasing ξ_o . The variation of the peak energy ($\epsilon_{\gamma,c}$) of the photospheric cascade is directly proportional to the variation of $\Gamma_{p,f}$ with ξ_o and increases with ξ_o . We have normalized these spectra by integrating the corresponding differential number fluxes from $\epsilon_{\gamma,c}$ up to the respective maximum energy ($\epsilon_{\gamma,\max}$) and equating to the respective total number flux in equation (19) with fixed $\xi_\gamma = 0.1$, the fraction of the total energy carried by the pions. The variation of the synchrotron peak energy ($\epsilon_{\gamma,m}$), in the range 330-400 keV, with ξ_o can be explained similarly. We have normalized the synchrotron spectra by integrating the corresponding differential number fluxes from $\epsilon_{\gamma,m}$ up to the energy $10\epsilon_{\gamma,m} \sim$ few MeV, the typical energy range for the *BATSE* and *BAT* detectors, and equating to the respective total number flux in equation (22). We have plotted an extension of the synchrotron spectra up to 1 GeV, in order to compare them with other spectral components.

The synchrotron spectrum does not extend very far above $\epsilon_{\gamma,m}$, for the parameters used here, from a calculation of the maximum electron Lorentz factor. The energy at which the Rayleigh-Jeans portion of the thermal photospheric photons start to dominate over the synchrotron spectrum is $\epsilon_\gamma \approx 2$ MeV for $\xi_o = 5$ and 10 curves in Figure 1. (For $\xi_o = 1$, the thermal component is small over the whole energy range.) Above this, besides the Comptonized photospheric cascade spectrum, there could also be an IC scattered component of the synchrotron photons (SSC), whose importance is characterized by the parameter $Y = [-1 + (1 + 4\epsilon_e/\epsilon_B)^{1/2}]/2 \approx 0.6$ for our present model. The corresponding minimum IC peak is $\gamma_{e,\min}^{\prime 2} \sim 4 \times 10^4$ higher than the synchrotron peak, at a photon energy $\epsilon_{\gamma,m,IC} \sim 10$ GeV. Hence an SSC component is not important in this case ($Y < 1$). Thus, at energies above which the synchrotron spectrum cuts off, the Comptonized photospheric cascade photon spectrum would be clearly distinguishable by *GLAST* (see Figure 1). Although for some choice of parameters an SSC contribution could become significant at energies $\gtrsim 10$ GeV, this is expected to be at energies much higher than the peak of the Comptonized cascade peak $\epsilon_{\gamma,c} \sim 300$ MeV. The maximum SSC photon energy, in the Thomson limit $\gamma_e' \ll m_e c^2/\epsilon_{\gamma,m}$, would be $\epsilon_{\gamma,IC} \ll m_e^2 c^4 \Gamma_i^2/\epsilon_{\gamma,m} \approx 300$ GeV. At energies well above ~ 10 GeV the two components (Comptonized photospheric cascade and SSC) may be hard to distinguish, but in the range of ~ 5 MeV - 10 GeV the Comptonized photospheric cascade should dominate. Below the peak $\epsilon_\gamma \lesssim \epsilon_{\gamma,c}$, the Comptonized photospheric cascade component is lower than the thermal photospheric peak, and at even lower energies it is also lower than the synchrotron component.

6. Discussion

If SGRBs are produced as a result of double neutron star or neutron star-black hole binary mergers, the neutron-rich outflow may result naturally in a high proton Lorentz factor $\Gamma_{p,f} \gtrsim 600$. Besides the usual non-thermal (e.g. internal shock) synchrotron spectrum, this implies the presence of a thermal photospheric component peaking around ~ 10 MeV. The n - p decoupling will lead to higher energy photons ($\gtrsim 0.1$ GeV) from neutral and charged pion decay cascades, and neutrinos ($\gtrsim 30$ GeV) directly from pion and muon decays. There may be additional X-ray emission when the neutron-decay proton shell with initial lower Lorentz factor impact with the decelerating proton shell initially moving with a high Lorentz factor (Dermer & Atoyan 2006). The afterglow light curves can also be affected by the neutron decay (Derishev, Kocharovsky & Kocharovsky 1999; Rossi, Beloborodov & Rees 2005). Here, we have concentrated on the prompt ($t \lesssim 2$ s) high energy (MeV to tens of GeV) signatures of neutron-rich outflows. For short bursts at $z \sim 0.1$ the ~ 50 GeV neutrinos are unlikely to be detectable with currently planned Gigaton Cherenkov detectors. However, the pion decay photons at ~ 60 GeV escaping from within a $\tau'_{\text{Th}} \sim 1$ skin-depth of the photosphere should be detectable with high area, high duty cycle Cherenkov detectors such as *Milagro*, at an estimated rate of 5 bursts per year. The pion decay photons created below the photosphere will result in a Comptonized cascade spectrum which, peaking in the range $\gtrsim 0.3$ GeV, dominates the non-thermal shock synchrotron-IC spectrum, and should be detectable with *GLAST*. Both the prompt GeV photon components discussed here are essentially contemporaneous with the usual MeV range short GRB prompt emission, $t_\gamma \lesssim 2$ s. Their detection or lack thereof could constrain the neutron content of the outflow and the nature of the short burst progenitors.

We thank the referee for comments which have helped us to improve the paper. Research supported in part through NSF AST 0307376 and NASA NAG5-13286.

REFERENCES

- Bahcall, J. N. and Mészáros, P. 2000, Phys. Rev. Lett., 85, 1362
- Barthelmy, D. L., et al. 2005, Nature 438, 994
- Belyanin, A. A., Derishev, E. V., 2001, A&A, 379:L25 (also astro-ph/0111558)
- Beloborodov, A. M. 2003, ApJ, 588, 931
- Dermer, C. D. and Atoyan, A. 2006, astro-ph/0601142

- Derishev, E. V., Kocharovsky, V. V. and Kocharovsky, VI. V. 1999, ApJ, 521, 640
- Derishev, E. V., Kocharovsky, V. V. and Kocharovsky, VI. V. 1999b, A&A, 345:L51
- Dingus, B. L. [Milagro collaboration] 2004, AIP Conf. Proc. 727, 131; also see <http://umdgrb.umd.edu/cosmic/technical%20description.htm>
- Fox, D. B., et al. 2005, Nature, 437, 845
- Gandhi, R., Quigg, C., Reno, M. H. and Sarcevic, I. 1998, Phys. Rev. D, 58, 093009
- Gehrels, N. and Michelson, P. 1999, Astropart. Phys., 11, 277
- Gehrels, N., et al. 2005, Nature, 437, 851
- Norris, J. P., Bonnell, J. T. 2006, ApJ(accepted), astro-ph/0601190
- Rossi, E. M., Beloborodov, A. M. and Rees, M. J. 2005, astro-ph/0512495
- Villasenor, J. S., et al. 2005, Nature, 437, 855
- Zhang, B. and Mészáros, P. 2004, Int. J. Mod. Phys., A 19, 2385

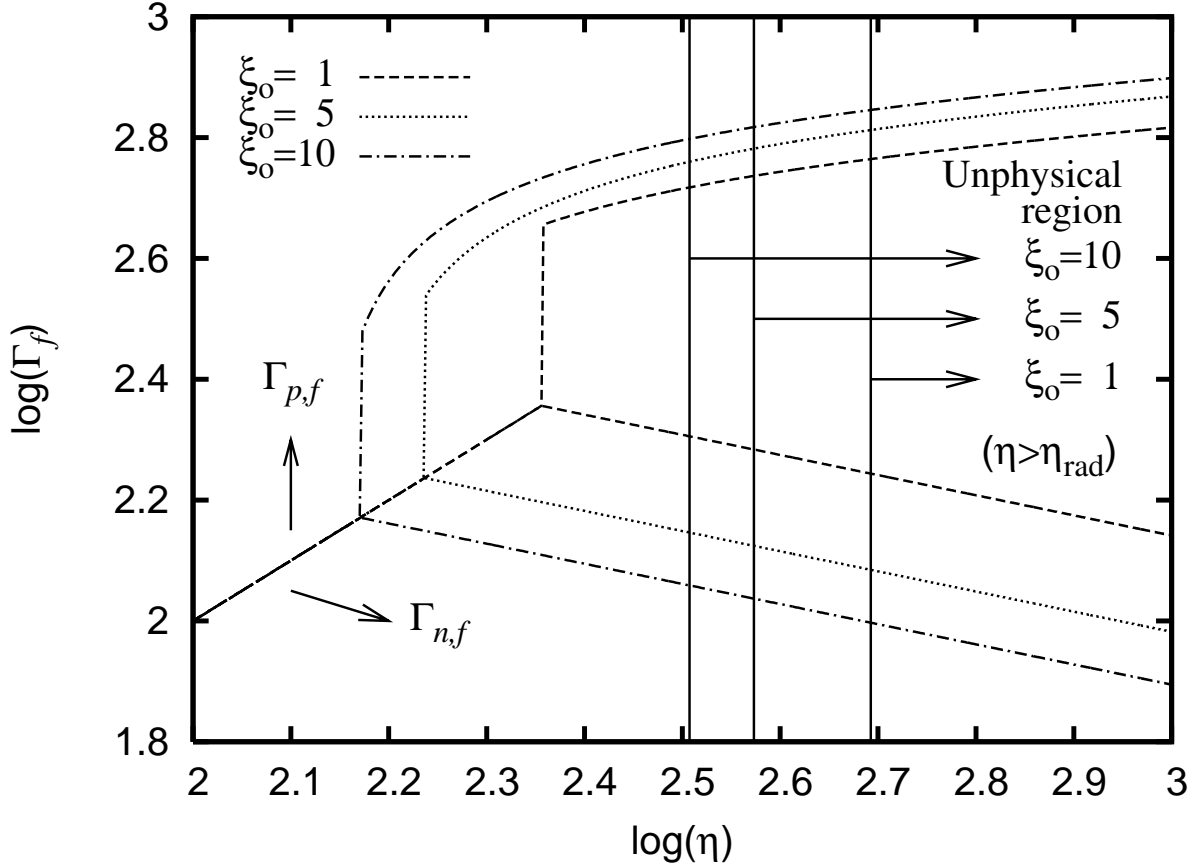


Fig. 1.— The final bulk Lorentz factor of the proton ($\Gamma_{p,f}$) and neutron ($\Gamma_{n,f}$) components, using equations (4) and (9) respectively, in the GRB jet outflow as functions of the baryon-loading parameter (η). The dashed, dotted and dotted-dash curves corresponds to the initial neutron to proton ratio $\xi_o = n'_n/n'_p = 1, 5$ and 10 respectively. The other parameters used are $L = 10^{50} L_{50}$ erg/s and $R_o = 10^6$ cm for all curves. For $\eta < \eta_{np}$, defined in equation (2), $\Gamma_{p,f} = \Gamma_{n,f} = \eta$ as shown by the single line. The protons and neutrons are held together in the outflow with leptons and photons in this case. For $\eta > \eta_{np}$ the protons and neutrons decouple as shown by the splitting of the curves at $\eta = \eta_{np} = 148, 172$ and 227 , and $\Gamma_{p,f} > \Gamma_{n,f}$. Note that the n - p decoupling takes place for lower η as ξ_o increases with other parameters fixed. The vertical lines at $\eta = 322, 374$ and 493 correspond to the limiting value of $\eta = \eta_{rad}$ defined in equation (10).

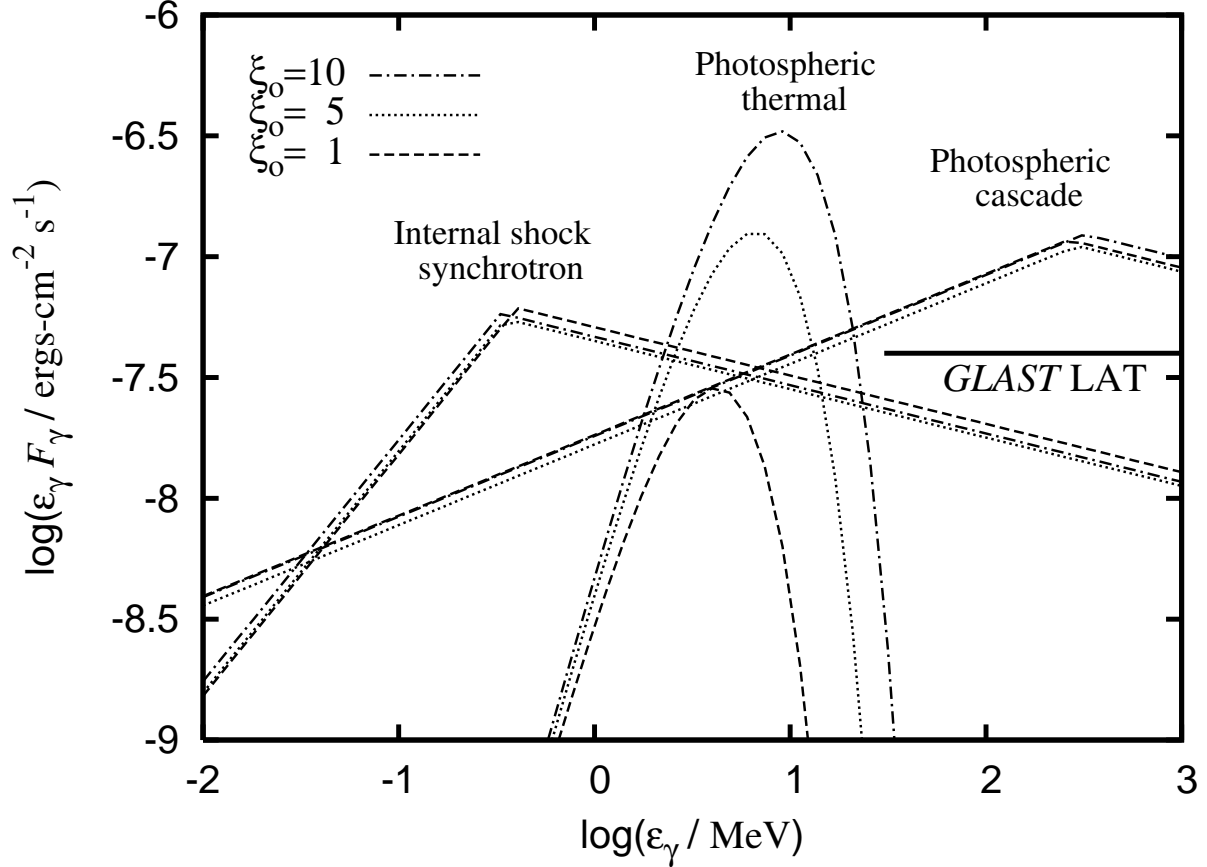


Fig. 2.— Photon spectra of the expected photospheric signals (thermal and IC cascade by pion decay electrons and photons) and the synchrotron spectrum from internal shocks, compared to the *GLAST* LAT sensitivity. The dashed, dotted and dotted-dash curves corresponds to the initial neutron to proton ratio $\xi_o = n'_n/n'_p = 1, 5$ and 10 respectively as in Figure 1. The other parameters used are $L = 10^{50} L_{50}$ erg/s, $R_o = 10^6$ cm and $\eta = 316$ for all curves. To calculate the internal shock synchrotron spectra we used a fixed variability time $t_v = 10^{-3}$ s. The peaks of the spectra are correlated with the final bulk Lorentz factor of the proton outflow: $\Gamma_{p,f} = 519, 572$ and 624 respectively for $\xi_o = 1, 5$ and 10 (see main text for more details).